Dynamics of CO_2^- radiation defects in natural calcite studied by ESR, electron spin echo and electron spin relaxation

2008 J. Phys.: Condens. Matter 20 255237

(http://iopscience.iop.org/0953-8984/20/25/255237)

J. Phys.: Condens. Matter **20** (2008) 255237 (10pp) doi:10.1088/0953-8984/20/25/255237

Dynamics of CO_2^- radiation defects in natural calcite studied by ESR, electron spin echo and electron spin relaxation

M Wencka[1], **S Lijewski and S K Hoffmann**

Institute of Molecular Physics, Polish Academy of Sciences, Smoluchowskiego 17, 60-179 Poznan, Poland

E-mail: mwencka@ifmpan.poznan.pl

Received 3 January 2008, in final form 22 April 2008
Published 22 May 2008
Online at stacks.iop.org/JPhysCM/20/255237

Abstract

ESR spectra were recorded in the X-band (9.6 GHz) and in the W-band (94 GHz) and electron spin relaxation was measured by electron spin echo (ESE) in the temperature range 4.2–300 K for radicals in natural calcite samples obtained from a cave stalactite and a dripstone layer. Four types of carbonate radical spectra and two sulfate radical spectra were identified and high accuracy g-factors were derived. Time and temperature behaviour of the spectra show that the dominating CO_2^- radicals are rigidly bonded or undergo free reorientations, whereas CO_3^-, SO_2^- and SO_3^- only undergo free reorientations. Below 200 K the free reorientations of CO_2^- are suppressed and a hindered rotation around single local axis appears. The ESE detected spectrum proves that the lines of free rotating radicals are homogeneously broadened, thus they cannot participate in electron spin echo formation. Spin–lattice relaxation data show that CO_2^- radicals are decoupled from lattice phonons and relax via local mode tunnelling motion between inequivalent oxygen positions of CO_2^- molecules. The tunnelling appears in two excited vibrational states of energy 71 and 138 cm^{-1}. Librational motions of CO_2^- molecules were detected by electron spin echo decay (phase relaxation) with energy 153 cm^{-1}. Two kinds of impurity hydrogen atoms were distinguished from ESEEM: in-water inclusions and water coordinated to the calcium ions.

1. Introduction

Calcium carbonates $CaCO_3$ (calcite, aragonite and vaterite) are common minerals in the natural environment. Calcite and aragonite based bio-minerals are formed in living organisms and provide an inspiration for the design of skeletal materials [1], hybrid composites and nanocomposites [2–5] and bone tissue engineering [6]. The quality of advanced calcite based materials can be influenced by defects and impurities occurring in the calcite structure. Calcite is the most thermodynamically stable rhombohedral form of $CaCO_3$ crystallizing in $R\bar{3}c$ ($Z = 6$) symmetry being a [111]-compressed NaCl-type lattice [7]. Large and high quality synthetic calcite crystals are not easily available and natural crystals of limestone and marble are still collected for optical applications. Calcite crystallizes also as cave deposits called dripstones or spelaeothems (stalactites, stalagmites). They appear as a result of the karst formation that is a solvation of the carbonate rocks by water containing CO_2 from the air or from the soil. The migrating water contains many impurities from inorganic materials in the penetrated rocks and clay minerals, and from organic materials dissolved during migration through the soil. The impurities can precipitate in the crystallizing calcite in the form of inclusions, or individual ionic or molecular impurities substituting host ions.

Moreover, the calcite crystals in natural conditions are permanently irradiated with ionizing α, β and γ ionizing irradiation from natural radionuclides existing in the surroundings. It results in free radical formation from host carbonate CO_3^{2-} molecular ions. The CO_2^- radicals with deficient O^-, CO_3^- with a deficient electron, and CO_3^{3-} with an excess electron, were identified by their ESR spectra. These radicals, especially CO_2^-, can have a very long lifetime in

[1] Author to whom any correspondence should be addressed.

calcite (of the order of 10^6 years at room temperature) and can be used for ESR dating in geochronology [8]. The ESR signal of CO_2^- radicals allows ESR dating up to 1 million years, which spans the time interval where ^{14}C-dating (5×10^4 years maximum limit) and K–Ar-dating (10^5 years minimum limit) are not applicable. The lifetime of stable carbonate radicals can be reduced by impurities (like water molecules or inclusions), which are diffusive in the calcite structure.

Except free radicals, the natural calcite crystals contain various paramagnetic ions like Mn^{2+}, Fe^{3+}, Zn^+ and Pb^{3+} that were identified by ESR [8]. The most common ionic impurity (up to a few per cent) in natural calcite is Mn^{2+}, which easily substitutes the Ca^{2+} ions. In this paper we present the results of ESR identification and characterization of paramagnetic defects and impurities in natural calcite samples. It should be noted that the ESR spectrum of a natural calcite strongly depends on the place where samples were collected. The spectra differ in the number and content of paramagnetic defects. A given ESR spectrum can be considered as a fingerprint of a specific place and the possibility of its application in ESR dating should be individually examined.

In this paper we present results of such an examination for natural calcite samples of stalactite and dripstone from two mountain caves and the data for synthetic calcite are also presented as the reference for the natural samples.

ESR spectra of various calcite samples have been widely studied and the ESR parameters (g-factors and hyperfine splitting) were determined from the X-band (9.5 GHz) measurements on powder samples as reviewed in [8]. ESR results for CO_2^- in naturally occurring calcite single crystal are also available [9–11].

Identification and separation of overlapping lines appearing in a powder X-band ESR spectrum is still a fundamental problem. This is crucial for ESR dating where radical concentration is determined from individual ESR lines. Therefore, in this paper except for the X-band spectra, the spectra recorded at high frequency (W-band, 94 GHz) are used. They have much higher resolution and thus allow separation of ESR lines from various radicals.

Dynamics of the crystal lattice, local dynamics of carbonate ions and diffusion processes influence stability, structure and lifetime of free radical centres, which can be crucial for ESR dating. However, less attention has been paid so far to the dynamics of radical centres in calcite. The dynamics can be recognized in the temperature behaviour of the ESR spectral parameter and in the line width behaviour [12]. Additional and more detailed information about radical dynamics can be obtained from electron spin echo studies of the electron spin relaxation (spin–lattice and phase relaxation).

Electron spin relaxation of free radicals in calcite has not been studied so far, except some preliminary experiments of low sensitivity performed at very low temperatures, which proved that an electron spin echo (ESE) signal can be generated [13, 14]. The ESE decay has been measured in aragonite only, and the phase memory time (spin–spin relaxation time) was determined as 1.58 μs at room temperature [15].

Electron spin–lattice relaxation of paramagnetic ions has been studied in calcite by pulse ESR methods for Fe^{3+} [16] and by ESR line width analysis for Pb^{3+} [17] showing that the ordinary two-phonon Raman processes govern the relaxation. Two-pulse and four-pulse electron spin echo FT spectroscopy has been used to explain the complexes of Cu^{2+} ions on the crystal surface of calcium carbonate mineral vaterite and calcite [18]. Dephasing of the electron spin echo (phase relaxation), which is very sensitive to molecular motions, has not been studied in calcite at all and the first results are presented in this paper.

The electron spin relaxation measurements were performed in the broad temperature range 4.2–300 K. Conclusions concerning electron spin coupling to the crystal lattice vibrations (phonons) and local mode vibrations of the radical molecule were drawn. Moreover, the Fourier transform of electron spin echo decay (ESEEM spectroscopy = electron spin echo envelope modulation spectroscopy) proved that in some calcite samples the impurity water molecules exist and stabilize the free radical structure.

2. Experiment

The samples were collected from two caves located in the Western Tatra Mountains: stalactite samples from Szczelina Chocholowska Cave (we will call these 'stalactite' in the text and figures) and dripstone layers from Czarna Cave (we will call these 'dripstone layer'). The material from Chocholowska Cave (having larger γ-ray background irradiation: 0.2 mGy y^{-1}) is older (about 50 thousand years—as we have dated by ESR), whereas that from Czarna cave (having lower background radiation: 0.063 mGy y^{-1}) is younger (it is dated on 4 thousand years). The caves differ also in rocks and in soil on the cave top through which dissolved materials migrate forming secondary carbonate deposits. The ESR spectra of the samples show a very weak signal from Mn^{2+} impurities but relatively strong signals from radical centres.

The collected samples were divided into smaller fragments, cleaned, crushed, ground in a ceramic mortar and sieved with a final grain size below 0.063 mm. Some samples were additionally γ-irradiated with doses of 400 Gy and 2.5 kGy for enhancement of the carbonate radical ESR signals. The CO_2^--radical concentration in irradiated samples was very small: 8×10^{13} and 2.6×10^{16} radicals g^{-1}, respectively. The concentration was determined by a double integration of the ESR spectra with respect to the Ultramarine Blue standard.

ESR and electron spin echo experiments were performed on a Bruker ESP 380E FT/CW X-band spectrometer operating at 9.8 GHz with a dielectric TE_{011} resonator and equipped with a helium flow Oxford CF935 cryostat. For enhancement of ESR spectra resolution the ESR radical spectra were additionally recorded in the W-band (94 GHz) with a Bruker E680 spectrometer at room temperature in Max-Planck Institute for Polymer Research at Mainz (Germany) and at low temperatures in EPSRC EPR National Service of Manchester University (United Kingdom). To avoid saturation effects the spectra were recorded at low microwave power of 1 mW in the X-band and 5 nW in the W-band.

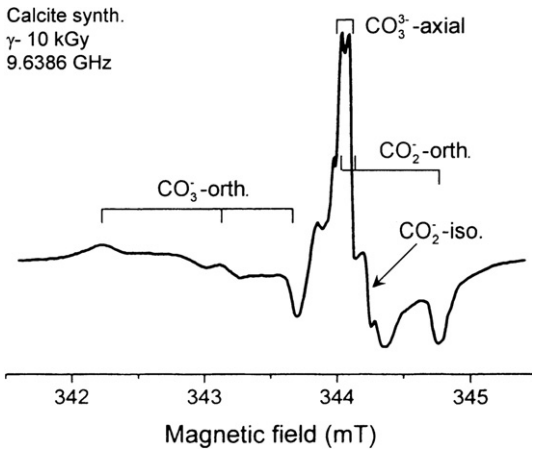

Figure 1. X-band ESR powder spectrum of synthetic calcite recorded at liquid nitrogen temperature after γ-irradiation with a dose of 10 kGy. Bars mark magnetic fields corresponding to g-factors of four types of carbonate radicals.

The electron spin relaxation was measured in the X-band using electron spin echo (ESE) signal. The ESE of CO_2^- radicals was excited by the pulse sequence 48–144–48 ns and the ESE was observed up to room temperature. The spin–lattice relaxation time T_1 was measured by the saturation recovery method with a 56 ns saturating pulse. Full saturation was achieved. The recovery after saturation had a trace of initial fast recovery and was bi-exponential for longer times. Both components are analysed in this paper. The dephasing time T_M of the spin precession motion was determined from the two-pulse ESE decay with two 48 ns pulses separated by a 144 ns time interval. The ESE amplitude decay was exponential and displayed modulation for some samples only.

3. Results and discussion

3.1. ESR spectra and radical identification

ESR spectra of the natural calcite samples derived from relatively young speleothem formations have relatively low intensity and generally display lines from Mn^{2+} ions in the form of sextets with splitting of about 9.4 mT. For enhancement of the radical ESR line intensity an additional ionizing irradiation (mostly γ-rays) is applied which can, however, produce new unstable radical species.

A reference spectrum for studies of natural calcite samples is the ESR spectrum of irradiated synthetic calcite, which is shown in figure 1. This spectrum, recorded after γ-irradiation with a dose of 10 kGy, shows signals from four types of carbonate radicals. The strongest signal arises from CO_2^- radicals having g-tensor of orthorhombic symmetry characterized by three g-factors ($g_x = 2.0031$, $g_y = 1.9973$ and $g_z = 2.0016$) [8]. Another CO_2^--centre displays a single weak symmetrical ESR line and is characterized by an isotropic $g = 2.0007$ value. CO_3^- radicals have an orthorhombic three-line spectrum lying on the low-field site, whereas CO_3^{3-} radicals display a strong axial-type spectrum characterized by two g-factors. They are stable at low temperatures only. Thus, the CO_3^{3-} radicals are not observed in our samples as can be recognized in the X-band spectra presented in figure 2.

The ESR spectrum of stalactite is weak, even for 400 Gy irradiated samples, and consists of relatively strong lines from orthorhombic CO_2^- radicals, weaker lines from isotropic CO_2^- and from SO_2^- impurities, and very weak lines from CO_3^- radicals at low field (see figure 2). The strong narrow line dominating the spectrum represents the signal from the E'-centre (electron localized at oxygen vacancy). This signal arises from the quartz tube, where the sample was placed, as is proved by a phase-reversed axial-type spectrum with

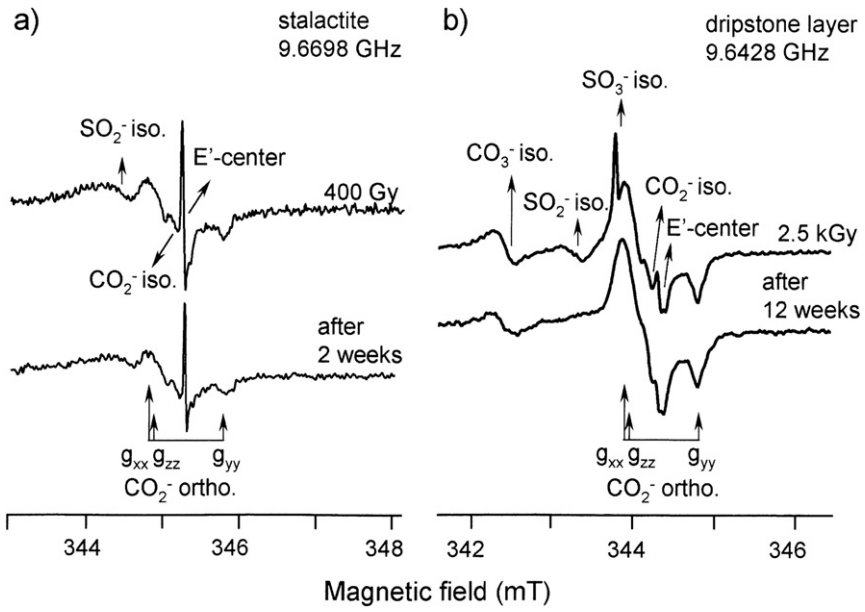

Figure 2. X-band ESR spectra of stalactite (a) and dripstone (b) recorded at room temperature after various doses of γ-irradiation (fresh samples) and after various time intervals of annealing.

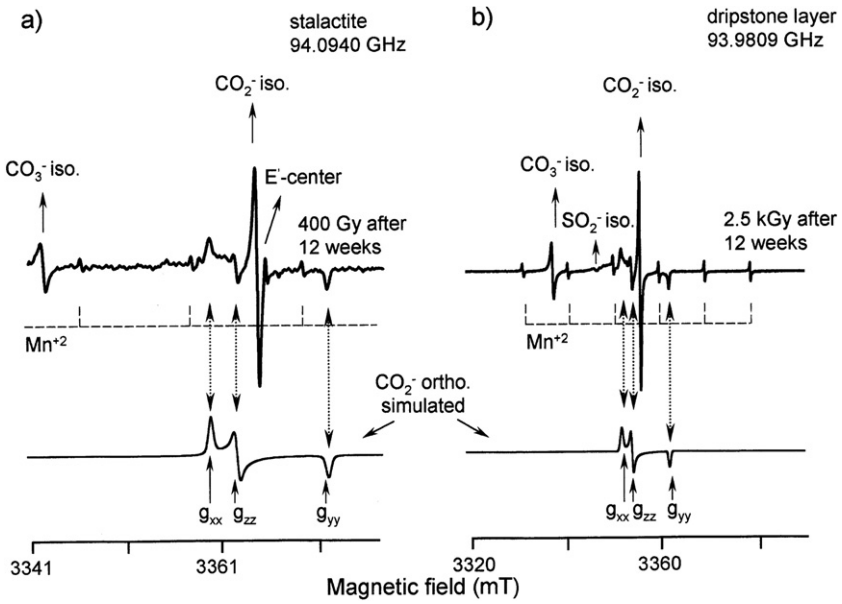

Figure 3. W-band (94 GHz) ESR spectra of stalactite (a) and dripstone (b) recorded at room temperature after treatment as in figure 2.

maximum amplitude at $g = 1.9999$. We have used the E'-centre peak as a field marker allowing an increase in accuracy of magnetic field measurements, which can suffer from small field gradient between the sample and the NMR magnetometer positions. The dripstone spectrum contains isotropic lines from SO_2^- and SO_3^- impurities. After a long annealing time (12 weeks) in darkness at room temperature the line from SO_3^- completely vanished and only a trace of SO_2^- lines remained. It means that the sulfate radicals are generated on diamagnetic impurity molecules during γ-irradiation and have short lifetimes compared to long-living carbonate radicals generated by natural radionuclides. The spectrum recorded after 12 weeks annealing is very stable with time. We have checked this for samples stored for 2 and 5 years at laboratory conditions. Samples displaying such a spectrum are suitable for ESR dating and were used in our pulsed ESR experiments.

Lines from CO_2^- radicals dominate the ESR spectra. These radicals are planar three-atomic molecules with the geometry and electronic structure described in [19]. Because of crystal symmetry the three differently oriented radical molecules, having the same g-factors, are observed in the angular dependence of the spectra in single crystals [10]. This means that any of the C–O bonding of the carbonate ion can be disrupted by the irradiation and the resulting radical molecule can be stabilized by lattice forces giving three orthorhombic ESR spectra at arbitrary crystal orientation. The existence of the isotropic spectrum of CO_2^- radicals, having a g-factor being the average of the three orthorhombic g-factors, indicates that some of the radicals are freely rotating and not stabilized in rigid positions. Thus, two types of CO_2^- radicals exist at room temperature–rigidly trapped and freely reorienting.

One can expect that except free reorientations a reorientation around a single x- or z- axis (the z-axis is perpendicular to the CO_2-plane, the x-axis is the two-fold symmetry axis of the radical) can appear producing an axial ESR spectrum with averaged g_y and $g_{z(x)}$ values. Such an axial-type spectrum would be located at the central part of the total spectrum and overlapped by the strong lines from orthorhombic and axial spectra. To check this we have recorded high-resolution ESR spectra in the W-band (94 GHz) at nW microwave power. The spectra recorded at room temperature are shown in figure 3. The spectra display the very well resolved orthorhombic spectrum of CO_2^- which was computer simulated for derivation of high accuracy g-factors. The isotropic lines are more intense as compared to the X-band spectra. Generally, isotropic lines dominate in W-band ESR powder spectra since an existing g-factors anisotropy leads to spreading of the spectra over a field range larger than the X-band, thus diminishing their amplitude [20]. There is no trace of the expected axial CO_2^- spectrum at room temperature but more visible are hyperfine lines of Mn^{2+}. The g-factors of radical species are summarized in table 1 where they are compared with previously published EPR results.

Table 1. ESR g-factors of free radicals in the stalactite and dripstone samples as calculated from the ESR W-band spectra. (Error in g-factors is ± 0.0001, for simulations $\pm 0.000\,05$.)

Radical	g_x	g_y	g_z	References
CO_2^--orthorhombic	2.003 15	1.997 10	2.001 70	This paper
	2.003 2	1.997 3	2001 6	[11]
	2.003 2	1.997 1	2.001 6	[41]
	2.003 2	1.997 4	2.001 5	[42]
CO_2^--axial	2.003 15	1.999 60		This paper
	2.003 1	1.999 4		[43]
	2.003 2	1.999 4		[9]
CO_2^--isotropic		2.000 7		This paper
		2.000 8		[42]
CO_3^--isotropic		2.011 6		This paper
		2.011 5		[44]
SO_2^--isotropic		2.006 2		This paper
		2.006 0		[45]
SO_3^--isotropic		2.003 1		This paper
		2.003 1		[46]

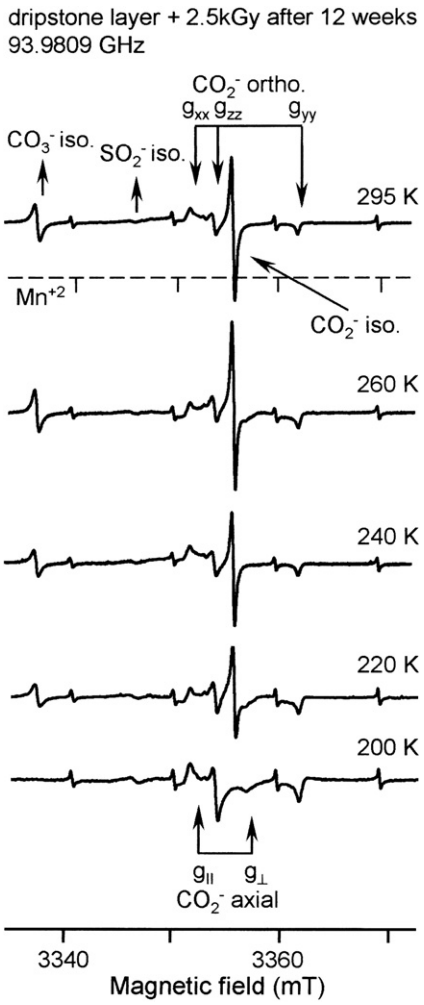

Figure 4. Temperature variations of the W-band spectrum of the dripstone layer sample displaying vanishing of the isotropic spectra of CO_2^- and CO_3^- with the simultaneous appearance of the axial CO_2^- spectrum below 220 K.

Summarizing, in stalactite and dripstone samples we observed carbonate radicals similar to those of irradiated synthetic calcite crystals. Except for the CO_2^- radical, the other radicals in the studied samples have isotropic ESR signals only, suggesting fast reorientations (tumbling) of the radical molecules. A proportion of the CO_2^- radicals (about 75% at 295 K) is stabilized in a rigid position by lattice forces. Moreover, ESR spectra show that both types of spelaeothems samples are contaminated by sulphates.

3.2. Temperature effects in ESR spectra

Temperature variations of ESR spectra were recorded in the W-band for the dripstone samples.

The results are shown in figure 4. Two effects are visible. The isotropic spectrum of CO_2^- gradually vanishes with decreasing temperature below 260 K and this is accompanied by the ESR line broadening. Simultaneously a new spectrum appears. Below 220 K, only this new spectrum exists and the isotropic signal disappears completely. The new spectrum has axial symmetry and g-factors ($g_\parallel$ and $g_\perp$) listed in table 1. These g-factors are related to the g-factor of the isotropic line and to the $g_{x,y,z}$ of the orthorhombic spectrum as $g_{\rm iso} = (2g_\perp + g_\parallel)/3 = (g_z + g_y + g_x)/3$. It means that the axial and isotropic spectra are the averaged form of the orthorhombic spectrum and that the reorientations appear between possible oxygen sites without significant radical molecule deformations. These results clearly show that at room temperature only a part of the CO_2^- radical molecules takes part in a tumbling-type motion or in random jumps around the local x, y, and z symmetry axes producing spatial averaging of the g-tensor components into the isotropic value. Below 220 K this motion becomes restricted and only reorientations around the x-axis exist.

The isotropic CO_3^- line gradually vanishes on cooling and disappears below 200 K. This could be due to a transformation into an anisotropic spectrum with the appreciable anisotropy resulting in a strong decrease in apparent spectral amplitude. It should be noted, that the isotropic signal of SO_2^--radicals is temperature independent, although these radicals are located at the same sites as carbonate CO_2^- radicals.

3.3. Electron spin relaxation

Electron spin relaxation, i.e. recovery of the spin system to the Boltzmann equilibrium after the excitation with the simultaneous recovery to spin precession motion with random phases, was measured using the electron spin echo (ESE) signal. Microwave pulses can generate ESE only for inhomogeneously broadened ESR lines. There are various causes of the inhomogeneous broadening [21]. One of these is the dipolar coupling to distant magnetic nuclei, which produces unresolved hyperfine lines. Because there is no magnetic nucleus of sufficient abundance in the $CaCO_3$ lattice, thus one can expect that the lines are homogeneously broadened and an ESE signals cannot be generated. The ESE signal, however, exists suggesting a g-factor distribution or the existence of an impurity atom with magnetic nuclei located near to the radical centre. When the ESR spectrum is recorded using echo-detected ESR (ED-ESR) method, one can recognize which radicals generate the ESE signal. In this method the ESE amplitude is recorded during a magnetic field sweep through the ESR spectrum and an absorption-type spectrum is obtained. Such spectra recorded both at X-band and W-band frequencies are shown in figure 5 where they are compared with corresponding CW-ESR spectra. The comparison clearly shows that the isotropic lines (see figures 1 and 3) are homogeneously broadened and do not participate in the ESE formation. The homogeneity of these lines is probably produced by fast radical dynamics. Thus, only the CO_2^--orthorhombic radical centres are responsible for the ESE signal. During relaxation measurements the external magnetic field was set to the central line of the orthorhombic spectrum and the ESE signal was excited with pulses having a bandwidth sufficient for the excitation of all the spins of the CO_2^- radicals.

3.3.1. Electron spin–lattice relaxation. The electron spin–lattice relaxation of CO_2^- radicals in calcite is relatively slow, allowing relaxation measurements up to room temperature where the relaxation rate reaches $1/T_1 = 10^5$ s^{-1}

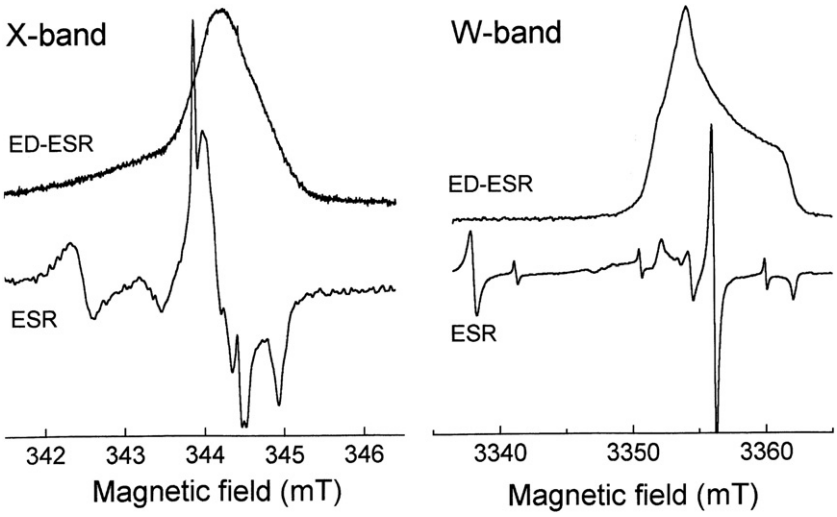

Figure 5. Comparison of continuous wave ESR spectra and echo-detected ED-ESR spectra of dripstone calcite. The homogeneously broadened line of freely rotating radicals and Mn^{2+} impurities do not appear in the ED-ESR spectra.

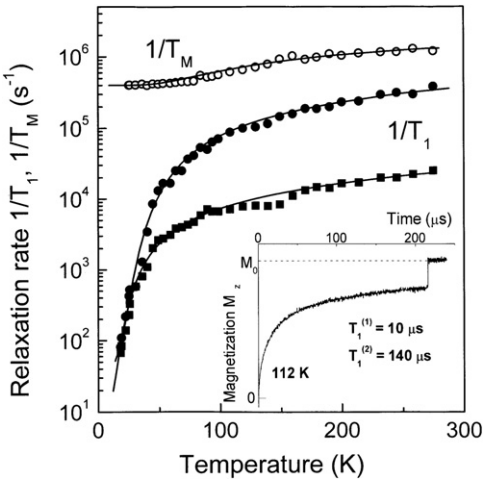

Figure 6. Temperature dependence of the spin–lattice relaxation rate $1/T_1$ for the fast and slow components of bi-exponential recovery of the spin system magnetization. The recovery at 112 K is shown in the inset with a jump to equilibrium value M_0 at long times.

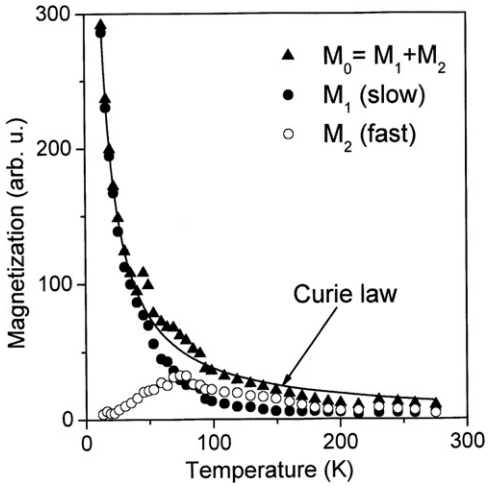

Figure 7. Temperature dependence of the fast (M_2) and slow (M_1) components of magnetization. The total magnetization M_0 of the spin system displays Curie law behaviour (solid line).

(see figure 6), whereas the relaxation of Fe^{3+} ions substituting calcium ions in calcite is very fast with $1/T_1 = 5 \times 10^7$ s^{-1} at 100 K and not measurable at room temperature [22]. It indicates that effective two-phonon Raman processes involving whole phonon spectrum and operating for paramagnetic ions are not active in a radical spin relaxation and another less effective relaxation process.

The recovery of magnetization to equilibrium after pulse excitation, observed by ESE amplitude, is bi-exponential in the whole temperature range. The recovery recorded at 112 K by using the standard Bruker routine 'Satrec' is shown as the inset in figure 6, with a characteristic jump to the equilibrium value M_0 for long times.

Because of the inevitable imperfection in the saturation recovery method resulting from a discrete pulse length (with 8 ns step) perfect saturation pulses cannot be achieved. As a result, the magnetization of the spin system (ESE amplitude) after saturation pulse is not equal to zero but has some initial value D. In such a case the bi-exponential recovery of $M_z(t)$ can be written as the three-variable (M_1, T_1 and T_2) equation:

$$M_z(t) = M_1\left[1 - \left(1 - \frac{D}{M_0}\right)\exp\left(-\frac{t}{T_{1\text{slow}}}\right)\right] + (M_0 - M_1)\left[1 - \left(1 - \frac{D}{M_0}\right)\exp\left(-\frac{t}{T_{1\text{fast}}}\right)\right] \quad (1)$$

where M_0 is the equilibrium magnetization value reached at limit $t \to \infty$, D is the initial M_z after pulse saturation and $M_0 = M_1 + M_2$. Equation (1) was used to fit the experimental data in the whole temperature range. The two relaxation rates $1/T_{1\text{slow}}$ and $1/T_{1\text{fast}}$ increase with temperature as shown by points in figure 6, and the two submagnetizations M_1 and M_2 vary in temperature as shown in figure 7. The temperature dependence of the total magnetization $M_0 = M_1 + M_2$ can

be approximated by the Curie law as shown by the solid line in figure 7. This confirms the validity of the fit with equation (1). The sum of two exponential functions of the recovery appears when the relaxing centre takes part in two mutually dependent (or–or) relaxation processes, but cannot take part in two relaxation processes simultaneously. In the latter case a product of exponents should appear. It should be noted that it was not possible to fit the experimental points of the temperature dependence with a single stretched exponential function as opposed to two exponents. It indicates that there is not a distribution of the spin–lattice relaxation time.

The mechanism of the spin–lattice relaxation is not related to the lattice phonons but is well described by the equation:

$$\frac{1}{T_1} = aT + b\,\mathrm{cosech}\left(\frac{\Delta}{kT}\right) \tag{2}$$

with parameters—for the slow relaxation rate (M_1-component): $a = 1.3(7)\ \mathrm{K}^{-1}\,\mathrm{s}^{-1}$, $b = 8.7 \times 10^3\ \mathrm{s}^{-1}$ and $\Delta_{\mathrm{slow}} = 71(5)\ \mathrm{cm}^{-1}$;—for the fast relaxation rate (M_2-component): $a = 3.7(6)\ \mathrm{K}^{-1}\,\mathrm{s}^{-1}$, $b = 2.53 \times 10^5\ \mathrm{s}^{-1}$ and $\Delta_{\mathrm{fast}} = 138(9)\ \mathrm{cm}^{-1}$. The small linear term aT gives an appreciable contribution below 10 K only and could result from a small non-uniformity in a spatial radical distribution in the calcite samples, as we have observed in some crystals [23]. Equation (2) is practically exponential in the temperature range $T < \Delta/k$ and it is a linear function of T for higher temperatures. The linear increase of the relaxation rate above 100 K was the first indication of the *cosech*-type behaviour.

The cosech(Δ/kT) dependence of the relaxation rate can be produced by a few mechanisms: (a) Murphy's mechanism involving a vibrational excitation of energy Δ with simultaneous spin flip [24, 25]; (b) cross-relaxation via exchange coupled pairs having singlet–triplet splitting Δ [26]; (c) two-level tunnelling states with tunnelling frequency Δ typical for disordered systems [27]. Mechanisms (b) and (c) can be excluded because the experimentally determined energy Δ is too high.

Two components of magnetization distinguished in the relaxation suggest that there are two spin subsystems (two types of radicals) involved in the relaxation. However, only CO_2^--orthorhombic radicals are able to produce the ESE signal and there is no cross-relaxation to other types of radicals, which should give temperature independent contribution to the relaxation rate. Two observations seem to clarify the situation: (1) $\Delta_{\mathrm{fast}} \approx 2\Delta_{\mathrm{slow}}$; (2) the fast component is practically equal to zero at 4.2 K and then grows reaching maximum value at about 100 K. At this temperature the thermal energy becomes comparable with Δ_{fast}. It clearly suggests that excitations to two excited vibrational levels are involved in the spin–lattice relaxation of CO_2^-. However, such excitations are not coupled to the spin, and thus cannot produce the relaxation directly. But, when a radical molecule is involved in reorientations between inequivalent potential wells, the jumps between the wells can be accompanied by a spin flop [28]. Indeed, the pre-exponential coefficient b in equation (2) is $8.7 \times 10^3\ \mathrm{s}^{-1}$ for the slow component and $2.53 \times 10^5\ \mathrm{s}^{-1}$ for the fast component. These frequencies are much lower than molecular vibration frequencies (being of order 10^{11}–$10^{13}\ \mathrm{s}^{-1}$) and are typical for tunnelling frequencies through a high potential barrier via a phonon-controlled tunnelling process [29]. Thus, the proposed model of the spin–lattice relaxation of CO_2^- involves tunnelling between inequivalent potential wells via two excited vibrational states. Tunnelling from the second excited state is faster but is still too slow for averaging of the g-factors and the CO_2^--orthorhombic radicals are visible as 'rigidly bonded' even at room temperature.

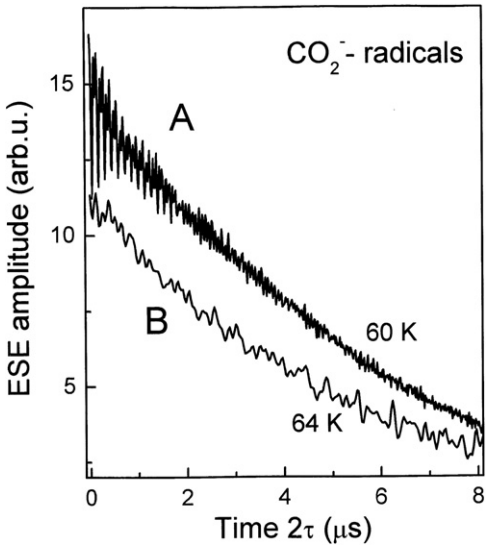

Figure 8. Electron spin echo amplitude decay at 60 K: A—modulated decay for freshly powdered dripstone samples; B—non-modulated ESE decay for stalactite samples and for aged dripstone samples.

3.3.2. Phase relaxation–electron spin echo dephasing. Although the samples of calcite from the two caves have identical electron spin–lattice relaxation behaviour, they differ in ESE dephasing (phase relaxation). This is visible in the electron spin echo amplitude decay presented in figure 8. The noisy but smooth decay B is observed for stalactite samples and for old dripstone samples (see section 2). For young dripstone samples, i.e. samples freshly prepared as fine powder from bulk materials, the decay A is observed. This decay is clearly modulated by dipolar interaction with the magnetic nuclei of atoms surrounding carbonate radicals. The modulation amplitude slowly decreases with time and after two years of ageing the modulation pattern vanished completely. The analysis of the modulation is presented in the section 3.3.3.

ESE amplitude $V(2\tau)$ decay depends on temperature but the decay is identical for all samples, i.e. it is free of modulation. The decay function is described by the equation:

$$V(2\tau) = V_0 \exp\left(-a\sqrt{\tau} - b\tau\right) \tag{3}$$

where τ is the inter-pulse interval. The first term in equation (3) dominates for temperatures higher than 150 K and is characteristic of spin diffusion i.e. a transfer of spin excitation energy between excited and non-excited spins [25, 30]. The spin diffusion is due to dipole–dipole flip–flops and thus is expected to be temperature independent in a rigid lattice. We

have found that the a-coefficient grows exponentially with temperature from $a < 0.02$ at helium temperature to about $a = 1.2$ at room temperature indicating that spin diffusion is accelerated by molecular dynamics [31]. The second term in the equation (3) is due to the instantaneous diffusion i.e. dephasing produced by the second microwave pulse [32], which perturbs dipolar coupling between excited spins. The instantaneous diffusion is temperature independent with $b = 0.2$.

The characteristic time of the ESE amplitude decay, called phase memory time T_M,can be calculated, for any decay mechanism characterized by coefficients m and k, from the decay equation $V(\tau) = V_0 \exp(-m\tau^k)$ as $T_M = (m)^{-1/k}$. However, when several mechanisms contribute to the ESE decay then the effective memory time can be determined as the time when the ESE amplitude ratio reaches $V(\tau)/V_0 = 1/e$ [23, 31]. The phase memory time T_M is of the order of 1 μs and the dephasing rate $1/T_M$ weakly increases with temperature as shown by the upper plot in figure 6. The temperature dependence of the dephasing rate is well described by the equation (solid line in figure 6)

$$\frac{1}{T_M} = \left(\frac{1}{T_M}\right)_0 + \frac{1}{T_1} + d\exp\left(-\frac{\Delta}{T}\right) \qquad (4)$$

where the temperature independent term $(1/T_M)_0 = 4.1 \times 10^5$ s^{-1} is the contribution from the instantaneous diffusion, the second term is the contribution from the spin–lattice relaxation processes. The last term describes temperature dependent broadening of the spin packets by motions of the radical molecule with $d = 1 \times 10^6$ s^{-1} and activation energy $\Delta = 220$ K $= 153$ cm^{-1}. The Δ can be considered as the barrier for the internal reorientations of the CO_2^- radical between potential wells, although the d-coefficient value suggests tunnelling motion by a phonon-controlled mechanism i.e. phonon induced excitation to a higher vibrational state with subsequent relaxation to the neighbouring potential well.

3.3.3. Electron spin echo envelope modulations (ESEEM spectrum). The modulated decay of the ESE shown as A in figure 8 can be described as a product of two functions: $V(\tau) = V_{\text{decay}} V_{\text{modulations}}$. A deconvolution gives the decay function discussed above and a pure modulation function $V_{\text{modulation}}$ that is shown in the inset of figure 9. The Fourier transformation of the modulation function gives the spectrum of modulating frequencies shown in figure 9. This is an ENDOR-type spectrum with peaks at frequencies characteristic for protons around the nuclear Zeeman frequency ν_H ($\nu_H = 14.715$ MHz in an external experimental field $B_0 = 345.6$ mT) and the sum of combination frequencies around $2\nu_H$ characteristic for two-pulse ESE experiments. There exists a doublet of peaks around the fundamental frequency ν_H with $\nu_1 = 14.710$ MHz and $\nu_2 = 15.625$ MHz and a doublet exists also around $2\nu_H$ with $\nu_3 = 29.420$ MHz $= 2\nu_1$ and $\nu_4 = 31.250$ MHz $= 2\nu_2$. The spectrum is confusing since the ν_1 and ν_2 cannot be assigned as a dipolar doublet from the proton–electron coupling i.e. as the fundamental ν_α and ν_β modulating frequencies [33] since then a single line at

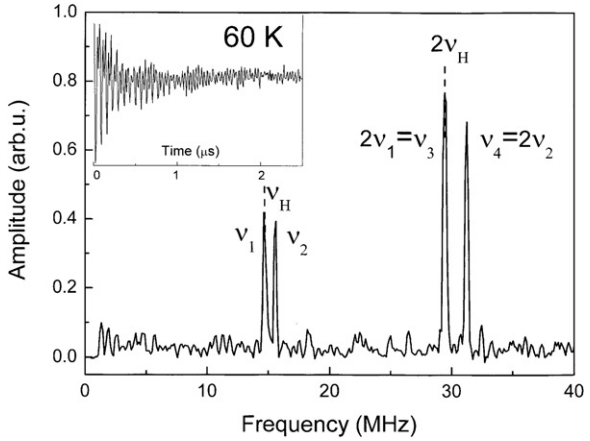

Figure 9. ESEEM spectrum (power FT-ESE of modulated decay A) at 60 K. Modulation is due to hydrogen impurities. The inset shows pure ESE decay modulation function.

($\nu_\alpha + \nu_\beta$) should appear. Instead of this, a doublet with double splitting $2(\nu_2 - \nu_1)$ exists. Thus, we conclude that the peak at $\nu_3 = 2\nu_1$ is a sum of the ν_α and ν_β frequencies which are not resolved in ν_1-peak. Similar occurs with the peak at $\nu_4 = 2\nu_2$. The non-resolved doublet of fundamental frequencies ν_α and ν_β indicates that the observed peaks are due to the distant protons (matrix protons) localized at distance larger than approximately 0.6 nm from a CO_2^- radical. The ν_1 frequency nearly coincides with ν_H and can be assigned as due to one kind of matrix protons whereas the peak at ν_2 is due to another kind of protons. The peaks are very narrow as expected when there is not a distribution of proton–electron splitting values and when the g-factor anisotropy is small. Another characteristic feature of the ENDOR-type spectrum is a higher amplitude of the combination peaks as compared with the fundamental peaks. Usually the opposite relation is observed, although we reported such an atypical amplitude relation in proton ESEEM spectrum of phenol-formaldehyde resin [34] and a possible explanation is discussed in the paper [35].

Protons in a natural calcite structure can appear as impurities introduced during the formation of dripstone layers. Many types of dissolved constituents sorb strongly to the calcite surface and can be incorporated into growing crystals. Protonated carbonate groups (bicarbonate) were identified by observation of the C–H coupling in double-resonance NMR cross-polarization spectra [36]. The presence of monolayers of hydroxyl species (−OH and H_2O) was observed by high-resolution x-ray reflectometry [37]. The existence of CO_2^- radicals surrounded by water molecules at distances 0.514, 0.535 and 0.502 nm has been observed by ENDOR and by general triple spectroscopy [38]. Irradiated natural calcite single crystals after γ-irradiation can show ESR lines from HCO_3^{2-} species [39], which we did find in our CW-ESR spectra.

We can conclude that the ESEEM spectrum indicated the existence of two kinds of water molecules in the freshly prepared dripstone samples. The signal at $\nu_1 \approx \nu_H$ can arise from weakly coupled protons of water inclusions, whereas the signal at ν_2 shifted by about 1 MHz from ν_H

can arise from crystalline water coordinated to Ca^{2+} ions as in monohydrocalcite $CaCO_3{\cdot}H_2O$ in a locally amorphous environment [40]. Different types of water molecules were observed also in ESEEM spectra of Cu^{2+} ions in calcium carbonate vaterite with a shift of about 0.75 MHz from the proton frequency [18]. Thus, ESEEM spectra give direct evidence of water impurities in calcium carbonates. Both types of water molecules gradually evaporate with storage time and after two years the proton peaks vanish completely in the ESEEM spectra.

4. Conclusions

Four carbonate and two sulfate free radicals were identified in the stalactite and dripstone layer samples. The identification was possible due to recording the ESR spectra in the W-band (94 GHz) where lines from various radicals differing in g-factors are well separated. This paper present the first ESR study of free radicals in calcite performed at high microwave frequencies with high precision g-factor determination. Our results show that it is not possible to make a high precision radical identification and determination of their spectral parameters from powder-type ESR spectrum at X-band frequencies. The W-band spectra recorded at broad temperature range 4.2–300 K allowed conclusions about the dynamics and thermal stability of the radical centres. We found that SO_3^- is not stable in our samples and disappears after 12 weeks of storage at normal conditions. The SO_2^- radicals are stable with time and are not affected by temperature, whereas the carbonate radicals are strongly influenced by cooling. The CO_3^- radicals giving single isotropic line in the ESR spectrum disappear with cooling below 200 K. The CO_2^- radicals are the dominant species in calcite and they appear in two forms at room temperature: as rigidly bonded molecules giving an orthorhombic ESR spectrum and as freely rotating molecules giving an isotropic ESR line. The free reorientations of CO_2^- become restricted below 220 K with a gradual transformation of the isotropic spectrum into an axial-type spectrum indicating that at low temperature there exists hindered rotation around a local molecular axis. These are the first observations of the transformation in powdered calcite samples. The dynamical averaging of the isotropic line is confirmed by the echo-detected ESR spectrum, which clearly shows that only the ESR lines of rigidly bonded CO_2^- are inhomogeneously broadened, thus only these species are excited in ESE experiments.

Additional information on radical dynamics has been delivered by electron spin relaxation studies. Spin–lattice relaxation data indicate that radical molecules do not participate in host lattice dynamics. It means that the radiation damage of the local crystal structure is large and the spin–phonon coupling is disrupted. Instead of participating in collective phonon motions the CO_2^- radicals have their own dynamics i.e. local modes of vibration which can be assigned as tunnelling between non-equivalent potential wells (incoherent tunnelling) via two excited vibrational states of energy 71 and 138 cm^{-1}. This can be treated as internal reorientations of radical molecule with jumps of oxygen atoms between three positions.

The dynamics of the whole CO_2^- molecule influences the dephasing of ESE and can be understood as a libration motion of the radical molecule which produces broadening of spin packets when the temperature increases. The librations are thermally activated with tunnelling between equivalent positions with an activation energy 153 cm^{-1}. The Fourier transform spectrum of modulated ESE decay shows that the natural calcite samples contain two types of water molecules. These are water inclusions and water molecules coordinated to the calcium ions.

The results presented show that the dynamics of CO_2^- radicals in calcite is rather complex but well recognized and should be taken into account when calcite based materials are considered and when samples are examined prior to ESR dating.

Acknowledgments

The authors would like to express their gratitude to Professor Gunnar Jeschke from the Max-Planck Institute for Polymer Research in Mainz (Germany) and Professor David Collison from EPSRC EPR at the University of Manchester (UK), in whose laboratory the W-band ESR measurements were carried out. The authors are indebted to Dr Yevhen Polyhach and Dr. Radosaw M Kowalczyk for technical assistance during the measurements, and to MSci. Ing. Ziemowit Fraczek for hardware and software service.

References

[1] Mann S 2001 *Biominaralization: Principles and Concepts in Bioinorganic Materials Chemistry* (Oxford: Oxford University Press)
[2] Ludwigs S, Steiner U, Kulak A N, Lam R and Melbrum F C 2006 *Adv. Mater.* **18** 2270
[3] Yue W, Park R J, Kulak A N and Meldrum F C 2006 *J. Cryst. Growth* **294** 69
[4] Mehta N and Hede S 2005 *Hypothesis* **3** 21
[5] Vollrath F and Knight D 2001 *Nature* **410** 542
[6] Vincent J 1990 *Structural Biomaterials* (Princeton, NJ: Princeton Uniwersity Press)
[7] Kikuchi C and Matarrese L M 1960 *J. Chem. Phys.* **33** 601
[8] Ikeya M 1993 *Application of Electron Spin Resonance—Dating, Dosimetry and Microscopy* (Singapore: World Scientific)
[9] McMillan J A and Marshall S A 1968 *J. Chem. Phys.* **48** 467
[10] Marshall S A and McMillan J A 1968 *J. Chem. Phys.* **49** 4887
[11] Marshall S A, Reinberg A R, Serway R A and Hodges J A 1964 *Mol. Phys.* **8** 225
[12] Wencka M, Hoffmann S K and Krzyminiewski R 2005 *Acta Phys. Pol.* A **108** 491
[13] Burkhardt J L 1959 *Phys. Rev. Lett.* **2** 149
[14] Wanlass K L and Wakabayashi J 1961 *Phys. Rev. Lett.* **6** 271
[15] Kohna H, Yamanaka C and Ikeya M 1994 *Japan. J. Appl. Phys.* **33** 5743
[16] Marshall S A and Nistor S V 1972 *Phys. Rev.* B **6** 1686
[17] Popescu F F and Grecu V V 1982 *J. Phys. C: Solid State Phys.* **15** 1547
[18] Schlosser P M, Wehrli B and Schweiger A 1999 *Geochim. Cosmochim. Acta* **63** 1955

[19] Carrington A and McLachlan A D 1967 *Introduction to Magnetic Resonance* (New York: Harper and Row) chapter 9.5
[20] Strzelczak G, Vanhaelewyn G, Stachowicz W, Goovaerts E, Callens F and Michalik J 2001 *Radiat. Res.* **155** 619
[21] Weil J A, Bolton J R and Wertz J E 1994 *Electron Paramagnetic Resonance: Elementary Theory and Practical Applications* (New York: Wiley) chapter 10.4
[22] Marshall S A, Nistor S V and Serway R A 1972 *Phys. Rev.* B **6** 1686
[23] Hoffmann S K, Hilczer W, Goslar J and Augustyniak-Jablokow M A 2001 *J. Phys.: Condens. Matter* **13** 7443
[24] Murphy J 1966 *Phys. Rev.* **145** 241
[25] Ichikawa T and Kurshev V V 1993 *J. Chem. Phys.* **99** 5728
[26] Hoffmann S K, Hilczer W, Goslar J, Kiczka S and Polus I 2002 *Phys. Chem. Chem. Phys.* **4** 4944
[27] Misra S K 1998 *Spectrochim. Acta* **54** 2257
[28] Ham F S 1972 *Electron Paramagnetic Resonance* ed S Geschwind (New York: Plenum) chapter 1, p 62
[29] Sussmann J A 1967 *J. Phys. Chem. Solids* **28** 1643
[30] Salikhov K M and Tsvetkov Y D 1979 *Time Domain Electron Spin Resonance* ed L Kevan and R N Schwartz (New York: Wiley) chapter 7
[31] Hoffmann S K, Goslar J, Lijewski S and Ulanov V A 2007 *J. Chem. Phys.* **127** 124705
[32] Kurchev V V and Ichikawa T 1992 *J. Magn. Reson.* **96** 563
[33] Dikanov S A and Tsvetkov Y D 1992 *Electron Spin Echo Envelope Modulation (ESEEM) Spectroscopy* (Boca Raton, FL: CRC Press)
[34] Hoffmann S K, Hilczer W and Hoffmann B 2002 *IEEE Trans. Dielectr. Electr. Insul.* **9** 316
[35] Kevan L 1979 *Time Domain Electron Spin Resonance* ed L Kevan and R N Schwartz (New York: Wiley) chapter 8.2.4
[36] Feng J, Lee Y J, Reeder R J and Phillips B L 2006 *Am. Mineral.* **91** 957
[37] Fenter P, Geissbuhler P, DiMasi E, Srajer G, Sorensen L B and Sturchio N C 2000 *Geochim. Cosmochim. Acta* **64** 1221
[38] Schramm D U and Rossi A M 1996 *Appl. Radiat. Isot.* **47** 1443
[39] Cass J, Kent R S, Marshall S A and Zager S A 1974 *J. Magn. Reson.* **14** 170
[40] Neumann M and Epple M 2007 *Eur. J. Inorg. Chem.* **14** 1953
[41] Rossi A and Poupeau G 1969 *Appl. Radiat. Isot.* **40** 1133
[42] Debuyst R, Bidiamambu M and Dejehet F 1991 *Nucl. Tracks* **18** 193
[43] Rossi A, Poupeau G and Danon J 1985 *ESR Dating and Dosimetry* (Tokyo: Ionics Publishing) p 77
[44] Debuyst R, Dejehet F and Idrissi S 1993 *Appl. Radiat. Isot.* **44** 293
[45] Serway R A and Marshall S A 1967 *J. Chem. Phys.* **46** 1949
[46] Eachus R S and Symons M C R 1968 *J. Chem. Soc.* A **45** 790